EUROGRAPHICS 2019 / P. Alliez and F. Pellacini
(Guest Editors)

Volume 38 (2019), Number 2

A Geometrically Consistent Viscous Fluid Solver with Two-Way Fluid-Solid Coupling

Supplementary Material

Tetsuya Takahashi[†] and Ming C. Lin[*,†]

[†]University of North Carolina at Chapel Hill
[*]University of Maryland at College Park

1. Statistics

Table 1 summarizes the simulation condition and performance for all the results. We note that the computational overhead for our geometrically consistent volume estimation is relatively small compared to the inconsistent volume estimation and the supersampling. Similarly, our strong two-way coupling requires almost the same amount of time for one-way and weak two-way coupling methods. Our position-correction method can better enforce the uniform distributions of particles leading to the smaller number of neighbor particles, and consequently, our method is at least 6 times faster than the distance-based position correction and is 2.5 times faster than the density-based position correction.

2. Derivation of Terminal Velocity for Solid Spheres

The analytical solution for the terminal velocity of a spherical solid in viscous fluids can be derived by equating the drag, buoyant, and gravity forces. When the Reynolds number $Re = 2\frac{\rho_f||\mathbf{V}||_2 r}{\eta}$ (ρ_f: fluid density, $\mathbf{V}$: solid velocity, r: solid radius, η: dynamic viscosity of fluids) is sufficiently low (typically $Re \ll 1$) and the domain is open boundaries (i.e., domain boundaries are far apart, and their influence to the solid is negligible), the drag force due to the viscosity $\mathbf{F}_d$ is $\mathbf{F}_d = 6\pi\eta r\mathbf{V}$ according to the Stokes' law. Since the sum of buoyant and gravity forces is $\mathbf{F}_g = \frac{4}{3}(\rho_s - \rho_f)\mathbf{g}\pi r^3$ (ρ_s: solid density, $\mathbf{g}$: gravity), the analytical terminal velocity $\hat{\mathbf{V}}^\infty$ is given by

$$\hat{\mathbf{V}}^\infty = \frac{2}{9}\frac{\rho_s - \rho_f}{\eta}\mathbf{g}r^2.$$

We note that this equation is valid only with a sufficiently low Reynolds number and open boundaries.

3. Two-Way Fluid-Solid Coupling

To validate the accuracy of the two-way fluid-solid coupling method compared to one-way coupling and weak two-way coupling in a wide range of viscosity values, we performed several experiments using a scenario, where a solid ball is falling inside of viscous fluids. In this experiment, we use $\eta = 1.0 \times 10^1, 1.0 \times 10^2, 1.0 \times 10^3, 1.0 \times 10^4$, and 1.0×10^5 kg$/(\mathrm{s}\cdot\mathrm{m})$, and visual results and solid velocity profiles are shown in Figures 1, 2, 3, 4, and 5, respectively.

Except for the case with viscosity $\eta = 1.0 \times 10^1$ kg$/(\mathrm{s}\cdot\mathrm{m})$ (Figure 1), where the Stokes' law and thus the analytical terminal velocity are not valid due to the high Reynolds number, the velocities of the solid balls simulated with strong two-way coupling are in good agreement with the analytical solutions. We note that while it requires a small amount of time for the simulated solid balls to reach the equilibrium, the solid ball for the analytical solution is directly moved from the beginning with the velocity given by the Stokes' law. As such, the height of the balls can be different for the simulation and analytical solution (e.g., in Figure 2).

By contrast, the velocities of solid balls simulated with one-way coupling and weak two-way coupling significantly deviate from the analytical solutions, unnaturally oscillate, and do not sufficiently reflect the differences of viscosity values. In addition, the incorrect behaviors of the solid ball with one-way and weak two-way coupling unnaturally deform the viscous fluid blocks (see the top of the blocks in the figures).

4. Position Correction

Figure 6 compares our position-correction method with methods using no position corrections and distance-based position corrections, and we use up to 50 iterations for our method and the distance-based position correction method. In this scene, a bulk of highly viscous fluids is successively compressed by circular plates with multiple holes.

The method with no position corrections can easily lose fluid volumes, and the viscous fluid does not reach the top. While the method with the distance-based position correction can preserve the volume better reaching the top, our method enables more volumes to reach the top. The color-coding for simulation particles also clarify that our method can resolve the compression of particles better compared to the distance-based position corrections. Additionally, we note that compared to our method, the distance-based position correction method can be more costly due to the large number of neighboring particles.

Table 1: *Simulation conditions and performance results. "Volume" represents which method is used for volume computation. "Coupling" represents a scheme used for the fluid-solid coupling. "Uniform" represents a scheme used to enforce the uniform distributions of particles, and the number of maximum iterations.* $t_{\text{vol}}, t_{\text{pres}}, t_{\text{visc}}, t_{\text{dens}}, t_{\text{rest}}$, *and* t_{total} *represent computation time in seconds per frame for volume fraction computation, pressure solve, viscosity solve, density solve, rest (e.g., data transfers, particle advection, velocity extrapolation), and total, respectively. * indicates figure numbers in the main paper. The computational time for the inconsistent volume estimation, supersampling, and consistent volume estimation are comparable (in orange). Our strong two-way coupling requires about the same amount of time for one-way and weak two-way coupling (in cyan). Our position-correction method is at least 6 times faster than distance-based and 2.5 times faster than density-based position corrections (in magenta).*

Scene	Grid resolution	Particles	η kg/(s·m)	Volume	Coupling	Uniform	t_{vol}	t_{pres}	t_{visc}	t_{dens}	t_{rest}	t_{total}
Fig. 1* (leftmost)	$128 \times 128 \times 128$	2,798.2k	1.0×10^3	Ours	One-way	Ours/3	11.2	2.2	26.0	16.2	10.1	65.7
Fig. 1* (left)	$128 \times 128 \times 128$	2,798.2k	1.0×10^3	Ours	Weak	Ours/3	10.1	2.0	20.4	15.3	8.6	56.4
Fig. 1* (right)	$128 \times 128 \times 128$	2,798.2k	1.0×10^3	Ours	Strong	Ours/3	8.9	1.8	20.4	9.0	5.7	45.7
Fig. 4* (left)	$192 \times 192 \times 192$	800.5k	1.0×10^1	Inconsistent	N/A	Ours/3	11.0	4.7	49.5	5.5	19.4	90.2
Fig. 4* (middle)	$192 \times 192 \times 192$	800.5k	1.0×10^1	Supersampling	N/A	Ours/3	11.0	5.7	47.1	5.3	19.9	89.0
Fig. 4* (right)	$192 \times 192 \times 192$	800.5k	1.0×10^1	Ours	N/A	Ours/3	12.5	5.2	51.7	5.4	19.6	94.5
Fig. 5* (left)	$144 \times 96 \times 96$	3,721.8k	up to 1.0×10^8	Ours	One-way	Ours/3	12.3	3.3	32.7	23.8	32.6	104.7
Fig. 5* (middle)	$144 \times 96 \times 96$	3,721.8k	up to 1.0×10^8	Ours	Weak	Ours/3	15.3	4.1	44.0	33.3	40.3	137.0
Fig. 5* (right)	$144 \times 96 \times 96$	3,721.8k	up to 1.0×10^8	Ours	Strong	Ours/3	11.2	3.0	42.2	21.3	26.7	104.4
Fig. 6* (middle)	$128 \times 128 \times 128$	up to 344.2k	1.0×10^3	Ours	N/A	Dist/50	12.9	0.6	5.9	75.6	3.8	98.8
Fig. 6* (middle)	$128 \times 128 \times 128$	up to 344.2k	1.0×10^3	Ours	N/A	Dens/50	15.3	0.7	7.0	29.7	4.7	57.4
Fig. 6* (right)	$128 \times 128 \times 128$	up to 344.2k	1.0×10^3	Ours	N/A	Ours/50	11.7	0.6	5.6	11.7	3.5	33.1
Fig. 7* (left)	$64 \times 128 \times 64$	2,405.0k	1.0×10^3	Ours	One-way	Ours/3	3.3	1.3	10.6	16.9	9.2	40.7
Fig. 7* (middle)	$64 \times 128 \times 64$	2,405.0k	1.0×10^3	Ours	Weak	Ours/3	3.0	1.2	9.6	16.2	3.5	33.5
Fig. 7* (right)	$64 \times 128 \times 64$	2,405.0k	1.0×10^3	Ours	Strong	Ours/3	2.7	1.1	9.7	7.3	2.9	23.7
Fig. 8* (left)	$128 \times 128 \times 128$	1,891.5k	1.0×10^8	Ours	N/A	None/0	43.4	6.6	38.6	0.0	71.5	160.1
Fig. 8* (middle)	$128 \times 128 \times 128$	1,891.5k	1.0×10^8	Ours	N/A	Dist/3	42.3	9.3	46.5	39.3	74.2	211.6
Fig. 8* (right)	$128 \times 128 \times 128$	1,891.5k	1.0×10^8	Ours	N/A	Ours/3	39.8	8.6	43.6	22.1	72.9	187.1
Fig. 9* (left)	$192 \times 384 \times 192$	up to 1,805.0k	1.0×10^1	Ours	Strong	Ours/3	152.1	13.5	81.8	11.5	82.8	341.8
Fig. 9* (middle)	$192 \times 384 \times 192$	up to 1,805.0k	1.0×10^2	Ours	Strong	Ours/3	129.6	11.0	95.4	9.4	69.9	315.2
Fig. 9* (right)	$192 \times 384 \times 192$	up to 1,805.0k	1.0×10^3	Ours	Strong	Ours/3	84.8	6.7	101.1	9.6	45.1	247.1
Fig. 10*	$128 \times 128 \times 128$	2,756.6k	1.0×10^2	Ours	Strong	Ours/3	30.0	5.5	70.8	28.4	43.5	178.2
Fig. 11* (left)	$128 \times 128 \times 128$	258.5k	3.0×10^2	Ours	Strong	Ours/50	17.1	1.5	11.9	16.1	10.8	57.4
Fig. 1 (left)	$64 \times 128 \times 64$	2,405.0k	1.0×10^1	Ours	One-way	Ours/3	4.4	1.8	9.7	21.0	12.5	49.5
Fig. 1 (middle)	$64 \times 128 \times 64$	2,405.0k	1.0×10^1	Ours	Weak	Ours/3	3.0	1.2	6.4	16.3	5.7	32.6
Fig. 1 (right)	$64 \times 128 \times 64$	2,405.0k	1.0×10^1	Ours	Strong	Ours/3	2.8	1.1	5.9	15.1	4.1	29.0
Fig. 2 (left)	$64 \times 128 \times 64$	2,405.0k	1.0×10^2	Ours	One-way	Ours/3	4.3	1.7	9.3	22.3	10.2	47.8
Fig. 2 (middle)	$64 \times 128 \times 64$	2,405.0k	1.0×10^2	Ours	Weak	Ours/3	3.0	1.2	7.6	16.0	3.5	31.3
Fig. 2 (right)	$64 \times 128 \times 64$	2,405.0k	1.0×10^2	Ours	Strong	Ours/3	2.8	1.2	7.7	8.1	2.9	22.8
Fig. 3 (left)	$64 \times 128 \times 64$	2,405.0k	1.0×10^3	Ours	One-way	Ours/3	3.3	1.3	10.6	16.9	9.2	40.7
Fig. 3 (middle)	$64 \times 128 \times 64$	2,405.0k	1.0×10^3	Ours	Weak	Ours/3	3.0	1.2	9.6	16.2	3.5	33.5
Fig. 3 (right)	$64 \times 128 \times 64$	2,405.0k	1.0×10^3	Ours	Strong	Ours/3	2.7	1.1	9.7	7.3	2.9	23.7
Fig. 4 (left)	$64 \times 128 \times 64$	2,405.0k	1.0×10^4	Ours	One-way	Ours/3	3.7	1.4	13.2	17.6	10.5	46.3
Fig. 4 (middle)	$64 \times 128 \times 64$	2,405.0k	1.0×10^4	Ours	Weak	Ours/3	3.1	1.1	11.3	16.8	3.7	36.0
Fig. 4 (right)	$64 \times 128 \times 64$	2,405.0k	1.0×10^4	Ours	Strong	Ours/3	2.6	1.0	11.8	6.9	2.7	24.9
Fig. 5 (left)	$64 \times 128 \times 64$	2,405.0k	1.0×10^5	Ours	One-way	Ours/3	3.6	1.6	20.0	18.0	9.3	52.5
Fig. 5 (middle)	$64 \times 128 \times 64$	2,405.0k	1.0×10^5	Ours	Weak	Ours/3	3.2	1.2	13.1	17.6	3.8	39.0
Fig. 5 (right)	$64 \times 128 \times 64$	2,405.0k	1.0×10^5	Ours	Strong	Ours/3	2.8	1.0	11.8	7.4	2.9	25.8
Fig. 6 (left)	$128 \times 128 \times 128$	1,891.5k	1.0×10^8	Ours	N/A	None/0	43.4	6.6	38.6	0.0	71.5	160.1
Fig. 6 (middle)	$128 \times 128 \times 128$	1,891.5k	1.0×10^8	Ours	N/A	Dist/50	45.7	10.5	54.7	538.6	87.1	735.5
Fig. 6 (right)	$128 \times 128 \times 128$	1,891.5k	1.0×10^8	Ours	N/A	Ours/50	39.7	10.2	48.3	190.9	78.8	367.8

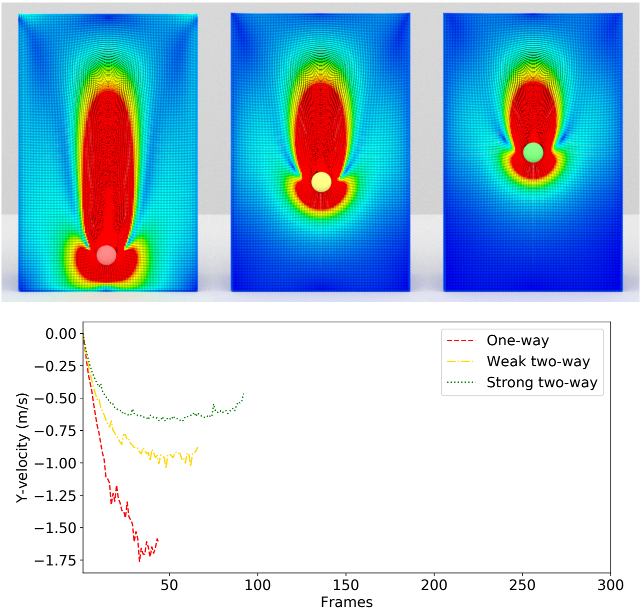

Figure 1: *A solid ball falling inside of fluids with viscosity* $\eta = 1.0 \times 10^1\ \mathrm{kg}/(\mathrm{s}\cdot\mathrm{m})$. *(Top) From left to right, one-way coupling, weak two-way coupling, and strong two-way coupling. Red, green, and blue particles represent large, medium, and small velocity magnitudes, respectively. (Bottom) Profile of the y-directional velocity of the solid balls. Note that due to the high Reynolds number, the analytical solution is not valid and thus the figure and plot for the analytical solution is excluded.*

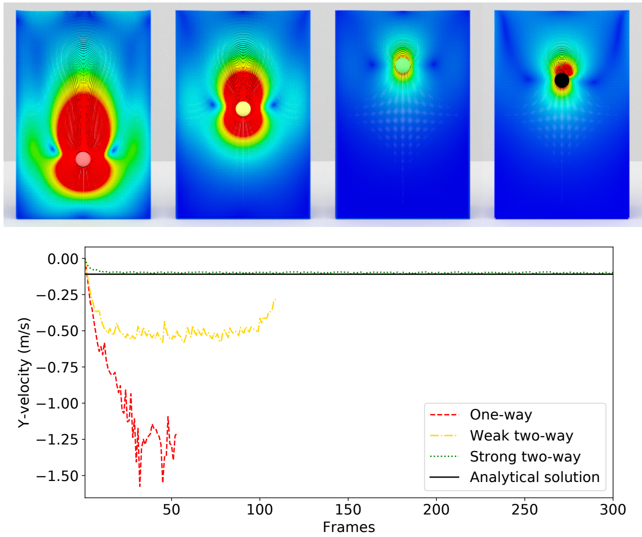

Figure 2: *A solid ball falling inside of fluids with viscosity value* $\eta = 1.0 \times 10^2\ \mathrm{kg}/(\mathrm{s}\cdot\mathrm{m})$. *(Top) From left to right, one-way coupling, weak two-way coupling, and strong two-way coupling. (Bottom) Profile of the y-directional velocity of the solid balls. Our strong two-way coupling gives solid velocities very close to the analytical solution while the solid velocities given with one-way and weak two-way coupling significantly deviate from the analytical solution.*

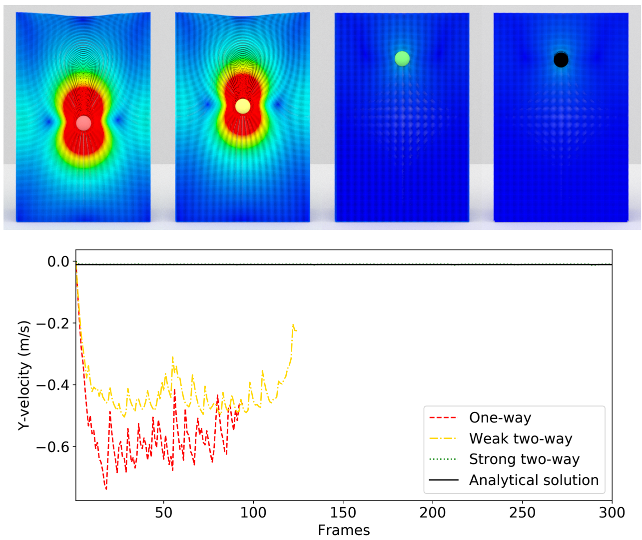

Figure 3: *A solid ball falling inside of fluids with viscosity values* $\eta = 1.0 \times 10^3\ \mathrm{kg}/(\mathrm{s}\cdot\mathrm{m})$. *(Top) From left to right, one-way coupling, weak two-way coupling, and strong two-way coupling. (Bottom) Profile of the y-directional velocity of the solid balls. Our strong two-way coupling gives solid velocities very close to the analytical solution while the solid velocities given with one-way and weak two-way coupling significantly deviate from the analytical solution.*

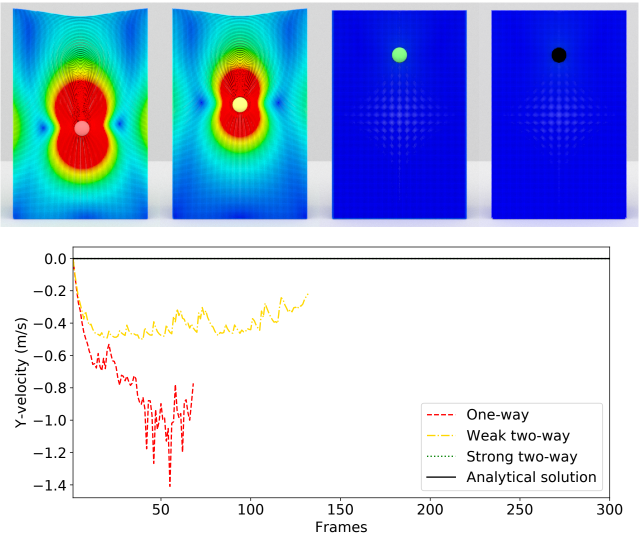

Figure 4: *A solid ball falling inside of fluids with viscosity values* $\eta = 1.0 \times 10^4\ \mathrm{kg/(s \cdot m)}$*. (Top) From left to right, one-way coupling, weak two-way coupling, and strong two-way coupling. (Bottom) Profile of the y-directional velocity of the solid balls. Our strong two-way coupling gives solid velocities very close to the analytical solution while the solid velocities given with one-way and weak two-way coupling significantly deviate from the analytical solution.*

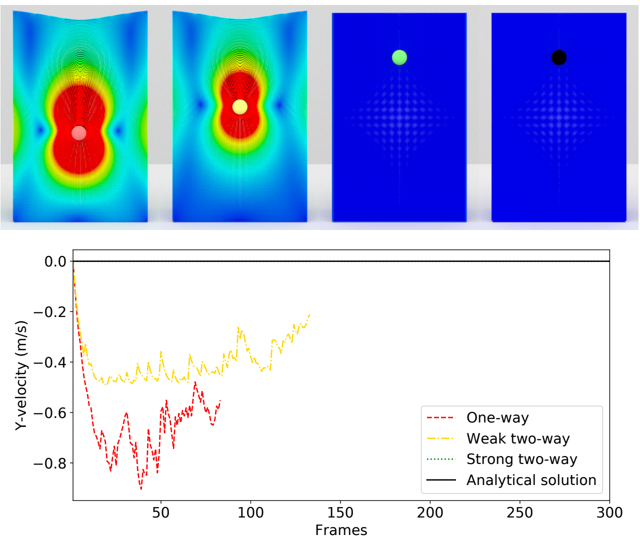

Figure 5: *A solid ball falling inside of fluids with viscosity values* $\eta = 1.0 \times 10^5\ \mathrm{kg/(s \cdot m)}$*. (Top) From left to right, one-way coupling, weak two-way coupling, and strong two-way coupling. (Bottom) Profile of the y-directional velocity of the solid balls. Our strong two-way coupling gives solid velocities very close to the analytical solution while the solid velocities given with one-way and weak two-way coupling significantly deviate from the analytical solution.*

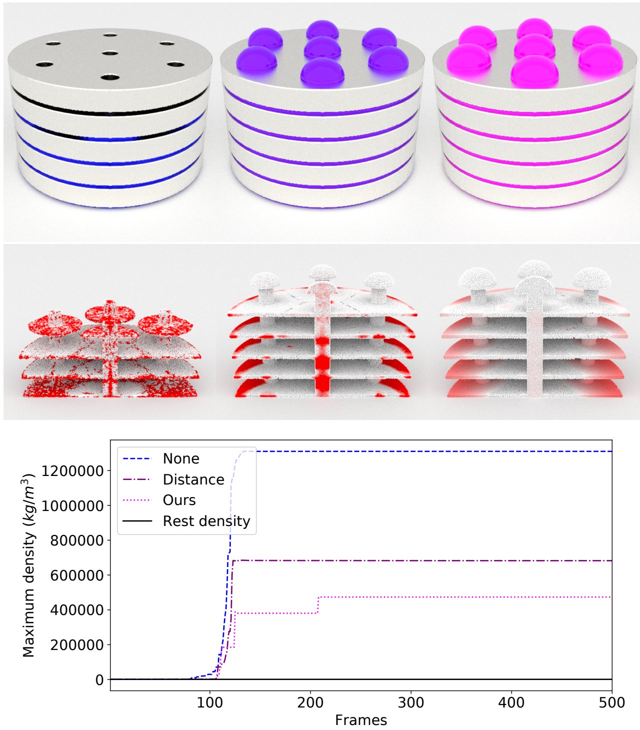

Figure 6: *(Top) A viscous fluid volume successively compressed by prescribed circular plates with several holes. From left to right, no position correction, distance-based position correction, and our method for surface rendering and particle view with color coding (white and red represent low and high densities, respectively). (Bottom) Profile of the maximum particle density, which indicates the inverse of local volumes. Compared to other approaches, our method preserves the density closer to the original one.*

5. Implementation Details on J

Given viscous stress $\mathbf{s} = (s_{xx}, s_{xy}, s_{xz}, s_{yy}, s_{yz}, s_{zz})^T$ defined on the staggered grid, the translational viscosity forces (F_x, F_y, F_z) applied from fluids to a rigid body can be written with grid indices i, j, k, control volumes V and voxel size Δx as

$$F_x = \sum_{i,j,k} (J_{xx,i,j,k} s_{xx,i,j,k} + J_{xy,i-1/2,j-1/2,k} s_{xy,i-1/2,j-1/2,k} + J_{xz,i-1/2,j,k-1/2} s_{xz,i-1/2,j,k-1/2}),$$
$$F_y = \sum_{i,j,k} (J_{yx,i-1/2,j-1/2,k} s_{xy,i-1/2,j-1/2,k} + J_{yy,i,j,k} s_{yy,i,j,k} + J_{yz,i,j-1/2,k-1/2} s_{yz,i,j-1/2,k-1/2}),$$
$$F_z = \sum_{i,j,k} (J_{zx,i-1/2,j,k-1/2} s_{zx,i-1/2,j,k-1/2} + J_{zy,i,j-1/2,k-1/2} s_{yz,i,j-1/2,k-1/2} + J_{zz,i,j,k} s_{zz,i,j,k}),$$

where

$$J_{xx,i,j,k} = \frac{-V_{i+1/2,j,k} + V_{i-1/2,j,k}}{\Delta x},$$
$$J_{xy,i-1/2,j-1/2,k} = \frac{-V_{i-1/2,j,k} + V_{i-1/2,j-1,k}}{\Delta x},$$
$$J_{xz,i-1/2,j,k-1/2} = \frac{-V_{i-1/2,j,k} + V_{i-1/2,j,k-1}}{\Delta x},$$

$$J_{yx,i-1/2,j-1/2,k} = \frac{-V_{i,j-1/2,k} + V_{i-1,j-1/2,k}}{\Delta x},$$
$$J_{yy,i,j,k} = \frac{-V_{i,j+1/2,k} + V_{i,j-1/2,k}}{\Delta x},$$
$$J_{yz,i,j-1/2,k-1/2} = \frac{-V_{i,j-1/2,k} + V_{i,j-1/2,k-1}}{\Delta x},$$

$$J_{zx,i-1/2,j,k-1/2} = \frac{-V_{i,j,k-1/2} + V_{i-1,j,k-1/2}}{\Delta x},$$
$$J_{zy,i,j-1/2,k-1/2} = \frac{-V_{i,j,k-1/2} + V_{i,j-1,k-1/2}}{\Delta x},$$
$$J_{zz,i,j,k} = \frac{-V_{i,j,k+1/2} + V_{i,j,k-1/2}}{\Delta x}.$$

Ignoring the grid indices for readability (as of now), the rotational forces F_{rx}, F_{ry}, F_{rz} can be written with positions of viscous stress defined on a grid $\mathbf{x} = (x, y, z)^T$ and the center of mass for the rigid body $\mathbf{X} = (X, Y, Z)^T$ as

$$F_{rx} = \sum \left((y - Y)(J_{zx} s_{xz} + J_{zy} s_{yz} + J_{zz} s_{zz}) - (z - Z)(J_{yx} s_{xy} + J_{yy} s_{yy} + J_{yz} s_{yz}) \right),$$
$$F_{ry} = \sum \left((z - Z)(J_{xx} s_{xx} + J_{xy} s_{xy} + J_{xz} s_{xz}) - (x - X)(J_{zx} s_{xz} + J_{zy} s_{yz} + J_{zz} s_{zz}) \right),$$
$$F_{rz} = \sum \left((x - X)(J_{yx} s_{xy} + J_{yy} s_{yy} + J_{yz} s_{yz}) - (y - Y)(J_{xx} s_{xx} + J_{xy} s_{xy} + J_{xz} s_{xz}) \right).$$

Since the viscous stresses are defined at different locations on the grid in the staggered manner, in practice, we compute the rotational forces above, e.g., for F_{rz} by

$$\begin{aligned} F_{rz} = \sum_{i,j,k} \Big(& (x_{i,j,k} - X) J_{yy,i,j,k} s_{yy,i,j,k} - (y_{i,j,k} - Y) J_{xx,i,j,k} s_{xx,i,j,k} \\ & + \Big((x_{i-1/2,j-1/2,k} - X) J_{yx,i-1/2,j-1/2,k} - (y_{i-1/2,j-1/2,k} - Y) J_{xy,i-1/2,j-1/2,k} \Big) s_{xy,i-1/2,j-1/2,k} \\ & + (x_{i-1/2,j,k-1/2} - X) J_{yz,i,j-1/2,k-1/2} s_{yz,i,j-1/2,k-1/2} \\ & - (y_{i,j-1/2,k-1/2} - Y) J_{xz,i-1/2,j,k-1/2} s_{xz,i-1/2,j,k-1/2} \Big). \end{aligned}$$

Similarly, we can compute F_{rx} and F_{ry}. Given $\mathbf{F} = (F_x, F_y, F_z, F_{rx}, F_{ry}, F_{rz})^T$ as the generalized six-dimensional viscosity forces for a rigid body, by extracting coefficients for the viscosity forces to assemble $\mathbf{J}$, we obtain the following relation:

$$\mathbf{F} = \mathbf{J}\mathbf{s}.$$